SAND2016-5689C

Automatic Fault Classification of Photovoltaic Strings Based on an In-Situ IV Characterization System and a Gaussian Process Algorithm.

C. Birk Jones*, Manel Martínez-Ramón‡,§ Ryan Smith†,
Craig K. Carmignani*, Olga Lavrova*, Charles Robinson*, and Joshua S. Stein*

*Sandia National Laboratories Solar PV & Grid Integration, Albuquerque, NM, USA.
‡Department of Electrical and Computer Engineering, University of New Mexico, Albuquerque, NM, USA,
§Universidad Carlos III de Madrid, Leganés, Madrid, Spain.
†Pordis LLC, Austin, TX, USA.

***Abstract*—Current-voltage (I-V) curve traces of photovoltaic (PV) systems can provide detailed information for diagnosing fault conditions. The present work implemented an in-situ, automatic I-V curve tracer system coupled with Support Vector Machine and a Gaussian Process algorithms to classify and estimate abnormal and normal PV performance. The approach successfully identified normal and fault conditions. In addition, the Gaussian Process regression algorithm was used to estimate ideal I-V curves based on a given irradiance and temperature condition. The estimation results were then used to calculate the lost power due to the fault condition.**

***Index Terms*—IV characterization, gaussian process algorithm, support vector machine, fault detection**

I. Introduction

Reliable operations of photovoltaic (PV) plants requires advanced monitoring of string level performance. Many PV arrays now include the monitoring of DC voltage and current at the combiner box level. This level of monitoring can increase the chances of detecting faults and has been discussed in past literature [1], [2], [3]. However, a more complete understanding of string level characteristics can be achieved through current-voltage (I-V) curve traces [4]. I-V curve measurements are more commonly performed by PV module manufacturers or in a laboratory setting. However, new products are now available that can be embedded into a PV array and used to collect module and string level I-V curves on demand. For example, in-situ module level I-V traces were performed by Quiroz *et al.* to test the impact of partial shading and increased series resistance effects [5].

The present work adds to the capabilities of an in-situ I-V curve tracing system by embedding automated, machine learning classification and curve estimation algorithms into a tracer device. The experiments used a model 140A string level I-V curve tracer device produced by Pordis LLC. Algorithms, such as a Support Vector Machine (SVM) and a Gaussian Process (GP), were used to classify behavior and estimate ideal curves based on the collected plane of array (POA) irradiance and module temperature.

This paper includes the following sections: methodology, results, and conclusions. The methodology describes the proposed approach to automatically classify and estimate I-V curve performance data using the SVM and GP algorithms. The section also provides a brief description of the I-V tracer system. The results section reviews the accuracy of the classification and regression algorithms. Finally, the conclusions section defines the key findings and highlights the focus for future work.

II. Methodology

The presented work implemented an in-situ I-V curve tracing system. The system measured I-V curve performance at defined times during the day and the results were stored in a local database. The data was reviewed, automatically, using SVM and GP algorithms that first classified the existing condition, and then estimated ideal I-V curve behavior at a given POA irradiance and module temperature. Classification was used to determine whether a PV string was performing well or experiencing fault behavior. The estimate of normal behavior was performed so that a potential loss of electrical power caused by a fault condition could be calculated.

The automated process, described in Figure 1, began with the presentation of curve and weather data to the SVM classification machine. The classifier determined whether the particular I-V curve was a fault or not. If a fault was not

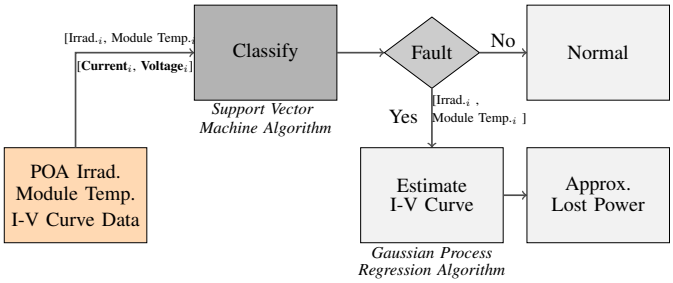

Fig. 1: The I-V curve data was evaluated in a multistep process. First, the SVM was used to classify the I-V curve as either a fault or normal condition. If a fault was discovered then an estimate of the I-V curve was determined by the GP algorithm. Finally, the lost power production was computed based on the comparison between the actual and estimated I-V curves.

detected, the curve was determined to be normal and the process ended. However, if the fault was found then the GP regression algorithm was presented with the POA irradiance

and module temperature values and estimated the potential I-V curve under. Based on this estimate the lost power was calculated by comparing it to the actual I-V curve data for the particular instance.

The proposed approach used SVM classification and GP regression algorithms. The algorithms were presented with a training data set, $D = ((x_i, y)|i = 1, ...n)$. The data set included the input feature vectors x and the expected value(s) y. The testing data set included the same x input features from training, but with different vector values (x_*). The testing outcome was the expected value y_*. The classification of the I-V curve data as normal or fault condition was performed by a SVM algorithm that considered the data set where x = ([irradiance$_i$,temp$_i$,voltage vector$_i$,current vector$_i$]) and y = (fault label$_i$). The approximation of the lost power performed by the GP regression algorithm used the data set where x = ([irradiance$_i$,module temp$_i$] and y = ([voltage vector$_i$, current vector$_i$]) to determine the most likely curve without a fault present. Once the most likely curve was estimated the difference between the actual and estimated was calculated to determine the power that was lost.

A. I-V Curve Classification

The classification of the I-V curves used the 250 current and voltage data points, measured by the Pordis 140A tracer, and the associated POA irradiance and module temperature to define the condition of the string as represented in Figure 2. In this experiment, the current and voltage curve data points

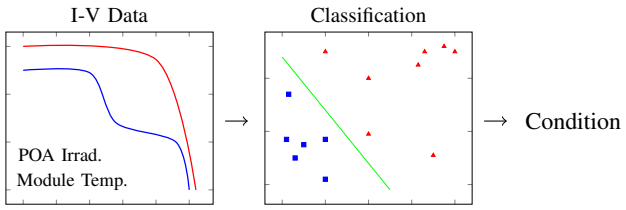

Fig. 2: The classification of the I-V characterization data was performed by a Support Vector Machine algorithm. The algorithm evaluated the I-V curve data at particular instances and classified the data as normal or a fault condition.

were normalized between zero and one and combined with the irradiance and module temperature to provide the inputs for the SVM. The associated conditions or classification for each data instance were defined as either a 0 for normal or 1 for fault. Then, during testing random I-V data, POA irradiance, and module temperature values were presented to the SVM algorithm.

The SVM algorithm, developed by Cortes and Vapnik [6], [7], can learn using supervised [8], [9] and unsupervised [10], [11] methods. The algorithm learns by separating different classes in a training data set with an optimal hyperplane.

In this case a classification algorithm was used, which is known as the Support Vector Classifier (SVC). It is a classification machine whose optimization criterion (for binary classification) can be written as

$$\begin{aligned} &\text{minimize } ||\mathbf{w}|| + C\sum_{n=1}^{N}\xi_n \\ &\text{subject to } y_n\left(\mathbf{w}^\top\mathbf{x}_n + b\right) > 1 - \xi_n, \\ &\xi_n > 0 \end{aligned} \tag{1}$$

where $y_n\left(\mathbf{w}^\top\mathbf{x}_n + b\right)$ is positive if sample $\mathbf{x}_n$ has been correctly classified. Therefore, slack variables (ξ_n) are used to account for the deviation of the response from its desired value ± 1. These slack variables are forced to be positive if $y_n\left(\mathbf{w}^\top\mathbf{x}_n + b\right)$ is higher than 1. In this case the corresponding slack variable is not included in the optimization shown in Eqn. (1). The sum of slack variables is minimized in the second part of the right side of Eqn. (1). This term is the empirical risk. At the same time, the criterion described in Eqn. (1), minimizes the complexity through the minimization of the norm of the parameters, where C is a free parameter that weights the trade-off between complexity and empirical risk.

The optimization can then be transformed into a non-constrained one using a Lagrange optimization with Lagrange or dual variables $\alpha_n \geq 0$ in the constraints. The result of the Lagrange optimization are as follow: First, the parameter vector becomes a linear combination of the patterns

$$\mathbf{w} = \sum_{n=1}^{N} y_n\alpha_n\mathbf{x}_n \tag{2}$$

Second, the values of the dual variables are optimized by solving the dual optimization problem

$$\text{minimize } \frac{1}{2}\boldsymbol{\alpha}^\top\mathbf{Y}\mathbf{K}\mathbf{Y}\boldsymbol{\alpha} + \sum_n \alpha_n \tag{3}$$

Here, $\boldsymbol{\alpha}$ is a column vector containing all dual variables, $\mathbf{Y}$ is a diagonal matrix containing the labels y_n, and $\mathbf{K}$ is a matrix containing all the dot products $\mathbf{x}_n^\top\mathbf{x}_n$ between patterns. The dual parameters are constrained to $0 \leq \alpha_n \leq C$, which is a free parameter that is defined through a cross validation process. The optimization is usually achieved by Sequential Minimal Optimization [12]. This formulation can be easily extended to have nonlinear properties by the use of the kernel trick. However, in this work, the linear SVC was used.

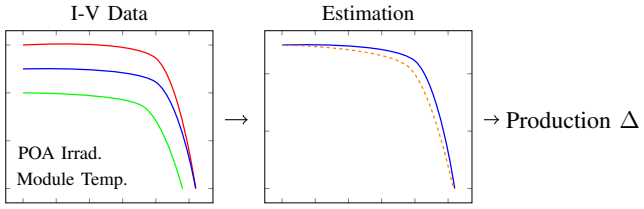

Fig. 3: The Gaussian Process Regression algorithm used past I-V curve data to learn good system behavior. It then was provided with previously unseen irradiance and cell temperature inputs and estimated the ideal I-V curve.

B. I-V Curve Estimation

The observations of inputs x_i (I-V data, POA irradiance, and module temperature) and outputs y_i (I-V curve estimates) were presented to the GP supervised learning algorithm as shown in Figure 3. The approach estimated the entire I-V curve. The estimated curve was then used to calculate the potential PV power production difference caused by the fault condition.

Typical learning algorithms assume that $y_i = f(x_i)$ for some unknown function f. For example, if the expected underlying function was linear then a least-squares method to fit a straight line could be applied. On the other hand, $f(x)$ may be quadratic or cubic, and therefore require other types of models. If this is the case, the GP algorithm provides a unique approach that does not relate $f(x)$ to a specific model. Instead it represents $f(x)$ by inferring a distribution over functions given a set of training data and then uses it to make predictions given a set of new data inputs [13].

The GP establishes a probabilistic model over the estimator as shown in Eqn. 4.

$$y_n = \mathbf{w}^\top \phi(\mathbf{x}_n) + \epsilon_n \tag{4}$$

The nonlinear transformation, $\phi(\cdot)$, was used to map the input into a Kernel Reproducing Hilbert Space. In this case, the Mercer theorem [14] was used by applying a dot product

$$k(\mathbf{x}, \mathbf{x}') = \phi(\mathbf{x})^\top \mathbf{\Sigma} \phi(\mathbf{x}') \tag{5}$$

between the transformed observations known as the covariance properties. $\mathbf{\Sigma}$ is a positive semidefinite matrix if and only if $k(\cdot, \cdot)$ is a positive semidefinite function.

The error or noise term ε is modelled through a Gaussian distribution $\mathcal{N}(0, \sigma^2)$ and is independent and identically distributed. Apriori over $\mathbf{w}$ is established with the form of a Gaussian random variable of zero mean and covariance matrix $\mathbf{\Sigma}_w$. The expression of the covariance $\mathbb{E}(y_n y_m | \mathbf{X})$ is

$$\begin{aligned} \mathbb{E}(y_n y_m | \mathbf{X}) &= \mathbb{E}\left((\mathbf{w}^\top \phi(\mathbf{x}_n) + \epsilon_n)(\mathbf{w}^\top \phi(\mathbf{x}_m) + \epsilon_m)\right) \\ &= \phi^\top(\mathbf{x}_n)\mathbb{E}(\mathbf{w}\mathbf{w}^\top)\phi(\mathbf{x}_m) + \mathbb{E}(\epsilon_m \epsilon_m) \\ &= \phi^\top(\mathbf{x}_n)\mathbf{\Sigma}_w \phi(\mathbf{x}_m) + \mathbb{E}(\epsilon_m \epsilon_m) \\ &= k(\mathbf{x}_n, \mathbf{x}_m) + \sigma^2 \delta(m - n) \end{aligned} \tag{6}$$

where $\mathbf{X}$ is a column matrix containing all input observations $\mathbf{x}_n$. Since $\mathbf{\Sigma}_w$ is positive definite, then $k(\cdot, \cdot)$ is a dot product and the covariance matrix can be written as

$$\mathbf{K}_{y,y} = \mathbf{K} + \sigma \mathbf{I} \tag{7}$$

where $\mathbf{K}$ is the matrix of kernel dot products between observations.

A predictive distribution can be constructed for a test sample $\mathbf{x}_*$ whose predicted output is $\mathbf{f}_* = \mathbf{w}^\top \phi(\mathbf{x}_*)$. This can be solved by computing the joint probability distribution of the training and test samples, which is a Gaussian with zero mean and covariance

$$\begin{pmatrix} \mathbf{K}_{*,*} & \mathbf{K}_{y,*} \\ \mathbf{K}_{*,y} & \mathbf{K}_{y,y} \end{pmatrix} \tag{8}$$

where $\mathbf{K}_{**} = k(\mathbf{x}_*, \mathbf{x}_*)$ and $\mathbf{K}_{*,y} = \mathbf{K}_{y,*}^\top$ is the row vector of all dot products $k(\mathbf{x}_*, \mathbf{x}_n)$. The *predictive* posterior over the new sample $\mathbf{x}_*$ given the training data can be computed using the Baye's rule, resulting in a Gaussian with mean and variance given by

$$\begin{aligned} \boldsymbol{\mu}_* &= \mathbf{K}_{y,*}\mathbf{K}_{y,y}^{-1}\mathbf{y} \\ \boldsymbol{\sigma}_*^2 &= \mathbf{K}_{*,*} - \mathbf{K}_{y,*}^\top \mathbf{K}_{y,y}^{-1}\mathbf{K}_{y,*} \end{aligned} \tag{9}$$

The GP then offers a posterior distribution over the prediction rather than a prediction alone. Its variance is reduced with respect to the variance of its prior in a quantity $\mathbf{K}_{y,*}^\top \mathbf{K}_{y,y}^{-1}\mathbf{K}_{y,*}$. The noise variance σ^2 and the kernel parameters are adjusted by optimization of the log-likelihood of the regressors y_n with respect to this parameter by taking derivatives over the parameters and applying a standard gradient ascent.

C. In-Situ I-V Characterization

I-V curve tracing systems currently available on the market are dominated by portable units capable of tracing individual modules or individual strings, depending upon the total capacity of the tracer. Research equipment extends the available equipment to include module-level tracers incorporating maximum power point tracking (MPPT) capabilities. No equipment previously existed which allowed automated tracing of I-V curves on multiple active, energy generating PV strings; Pordis developed an I-V tracing system capable of achieving in-situ measurements of active systems, thus enabling the real-time implementation of a GP algorithm for fault classification experiments.

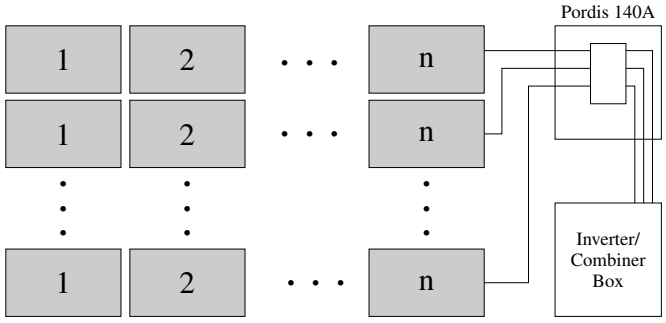

Fig. 4: The test array connects each string to the Pordis I-V Characterization System and then to the combiner box before connecting to the inverter.

The present work used a Regional Test Center (https://rtc.sandia.gov/) PV array as a test-bed for the in-situ I-V characterization and fault classification experiments. The array was constructed facing due south and had five strings as shown in Figure 4. Each of the strings connected to the Pordis LLC I-V tracer system. This system, known as the model 140A I-V curve tracer, was designed to be inserted into an array between the strings and the combiner box. The system incorporates a capacitive load with full string isolation during trace execution and has the capability to accommodate eight strings of up to 15A and 1000V per string for an overall system-level capacity of 120kW [15].

The 140A was designed as an in-situ tracer, which means that it may remain connected to the array at all times without impacting normal operations. It could efficiently perform I-V traces in-situ with the array because of a unique hybrid switch circuitry. Disconnecting an active, energy-generating string requires the switch operation to occur while the string is at the operating point as determined by the inverter, often the maximum power point (MPP). With crystalline silicon modules this could require switching a string operating at 750V and 13A. Common practice would accomplish this task using electromechanical devices designed to switch the full voltage and current; these devices are often physically large or must incorporate expensive inert gas or vacuum shielding to reduce arc-induced degradation of the contacts. The hybrid switch implemented in the 140A allows inexpensive components to achieve full-power switching without the need for additional shielding (vacuum or gas), and effectively eliminates limited lifetime due to contact carbonization. Power dissipation due to the additional circuitry was minimal.

The switch circuitry provided a low resistance path though the device during periods of normal energy production. Trigger events, defined in the user interface, commanded the I-V characterization sweeps for each string at predefined instances throughout the day. When triggered, the tracer isolated and redirected the selected string to the load portion of the device, a I-V trace was performed, and then the string was switched back into the array; the duration of the entire tracing cycle was less than 100ms. Additionally, the hybrid switch circuitry incorporated in the tracer did not trip the high-frequency arc fault detection nor the ground fault detection of the inverter used in the experiments. The results from each of the string I-V traces were stored in a database located in the tracer system and could be viewed through a web-interface. The GP algorithms accessed the I-V data automatically and provided feedback to the user immediately after the I-V trace tests were performed.

III. Results

The classification and regression algorithms were able to accurately determine fault conditions and estimate I-V curve performance for given module temperatures and POA irradiance. The classification results, described in Section III-A, indicated that the SVM algorithm could identify normal and fault conditions well. Also, the GP regression algorithm was also able to estimate the normal I-V curve behavior accurately (Section III-B). Therefore, it was able to determine a realistic estimate of the lost electrical power caused by the fault condition. For example, Section III-C considered the power lost due to a fault condition that degraded the overall string voltage.

A. Classification

The SVM classifier was linear, and a free parameter C value equal to 100. The algorithm trained and tested with data vectors $\mathbf{x}_i$ constructed by the concatenation of POA irradiance, module temperature, and I-V curve data vectors. The expected output of the classifier was binary and intended to discriminate the data produced by normal behavior from the data produced by abnormal behavior.

The algorithm was presented with 86 normal and 21 fault training data points. The data points included the I-V curve vectors and their respective POA irradiance and module temperature. Then, the trained SVM algorithm was presented with 324 new, previously unseen data points that had 242 normal and 82 fault conditions.

It was able to differentiate between normal and abnormal current and voltage behavior as shown in Figure 5. The

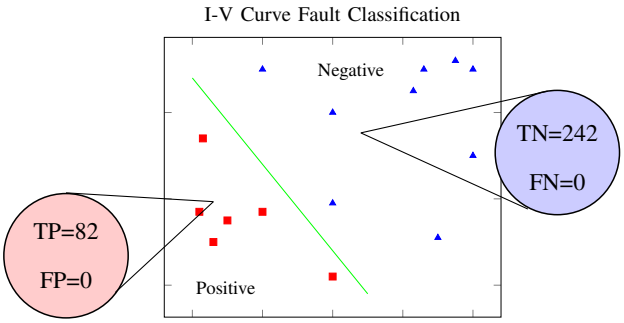

Fig. 5: The Support Vector Machine applied to this set of data resulted in 82 true positive (TP), 0 false positives (FP), 242 true negatives (TN), and 0 false negatives (FN).

algorithm identified 82 True Positive (TP) fault conditions without producing a single False Positive (FP). It also correctly identified 242 True Negative (TN) and zero False Negatives (FN). This resulted in a perfect false positive rate of 0% and a true positive rate of 100% for the given data set.

B. I-V Curve Estimation

The GP regression algorithm provided an estimate of current and voltage for an I-V curve by considering POA irradiance and module temperature as shown in Eqn. 10. The experiment implemented a squared exponential kernel shown in Eqn. 11.

$$[\text{Current, Voltage}] = f(\text{POA Irrad., Module Temp.}) \quad (10)$$

The algorithm was trained in an on-line learning manner. This approach meant that the training data grew as more data was

$$k(\mathbf{x}, \mathbf{x}') = \exp(-\gamma||\mathbf{x} - \mathbf{x}'||^2) \quad (11)$$

collected. For instance, the first estimation was based on a single training sample, the second estimation was based on two training data points, and so on. The estimation process began at training sample one and ended at sample 96. Therefore, 96 I-V curve estimates were calculated in the present work. The results indicated a highly accurate estimation of the I-V curves at different conditions.

The algorithm was able to accurately estimate I-V curve performance for a wide spectrum of POA irradiance (200-1000W/m^2) and module temperature (20-60°C) conditions. The actual and estimated voltage and current values for the I-V

curves were plotted against each other in Figure 6. The voltage estimates had a very strong linear relationship with the actual values. The linear fit line had a slope of 1 and an intercept of 0.36. Overall, the estimated current values were similar to actual. The linear fit line had a slope of 1 and an intercept close to zero. However, there were five curve estimates where the current was slightly higher or lower than the actual values. This is evident in the actual versus estimated plot for current in Figure 6.

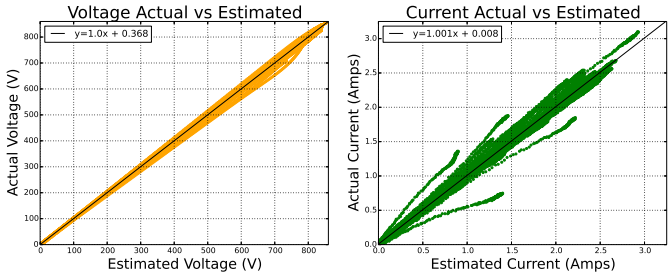

(a) The linear fit line for the voltage data had an intercept of 0.36 and a slope of 1.0.

(b) The linear fit line for current had an intercept less than 0.01 and a slope of 1.0.

Fig. 6: Actual versus estimated plots for the I-V curve data

The maximum power point calculated from the estimated I-V curves provided an accurate representation of power. The actual and estimated electrical power from the 96 I-V curves are plotted against each other in Figure 7. The plot shows that the estimates produced by the GP algorithm had a strong linear relationship with the actual values. The linear fit line had a

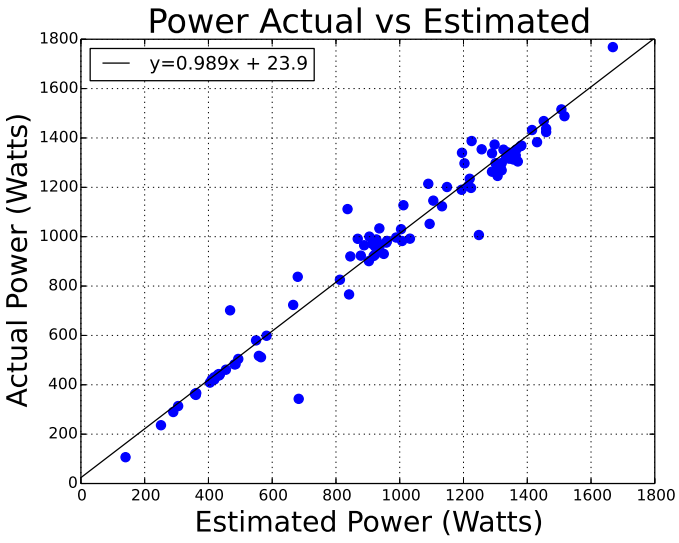

Fig. 7: Actual versus the Gaussian Process estimated string level power. The linear fit line shows that the estimate had a strong linear relationship with the actual data. The slope was close to 1 at 0.98 and the intercept was relatively low at 23.9.

slope close to 1 at 0.989 and an intercept at 23.9. The estimated power values were then used to determine the potential loss caused by a fault condition.

C. Fault Condition

The present work collected and reviewed I-V curve data from the four strings in a PV array. The classification and I-V curve estimation discovered that string 2 was underperforming. This was evident in the I-V curve results shown in Figure 8 where string 2 had degraded voltage output compared to the GP estimate and the actual results from string 1. The GP estimate and string 1 I-V curve results were very similar. The fault condition discovered in string 2 caused a decrease

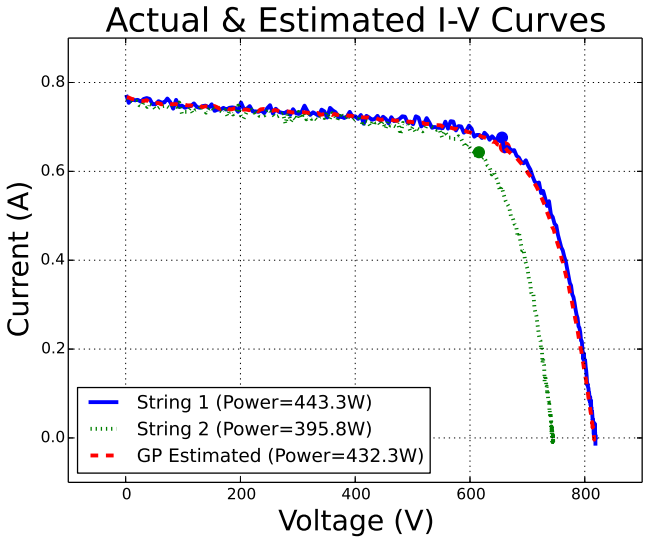

Fig. 8: String 1 and 2 I-V curves results compared to the Gaussian Process estimate. The I-V curve produced by string 1 had a very similar behavior to the Gaussian Process results. However, the I-V curve from string 2 was much different and was estimated to be producing about 38 watts less than desired.

in power. This decrease in power could be estimated by comparing the GP results with the actual I-V curve. For example, the I-V curves shown in Figure 8 had an estimated power of 395.8 Watts and 432.3 Watts for string 2 and the GP respectively. For this instance, the string was producing about 38 Watts less then it should be if it were not in a fault condition.

Further investigations into the cause of the degraded voltage revealed that a single module was underperforming and therefore activated the bypass diode. The damaged module had significant hotspots that caused it to heat up considerably as shown in the infrared (IR) image in Figure 9. In comparison, the IR image in Figure 10 shows a module that was not damaged and had no significant hotspots. The I-V tracer and automated classification and estimation tool was able to quickly identify this fault condition.

IV. Conclusion

Advanced PV system monitoring such as in-situ IV curve monitoring provides good information about PV system performance. However, operators may not have time to look

through and review every I-V curve produced. Therefore, an automatic machine learning algorithm such as the SVM classifier and GP regression proposed in this work can provide valuable information. The SVM classifier could automatically alert operators of fault conditions. The GP regression algorithm can provide a detailed comparison of the actual I-V curve with an ideal curve. This comparison could provide operators with a sense of how much power was lost due to the fault condition. This information could be valuable for operators so that they can prioritize maintenance activity.

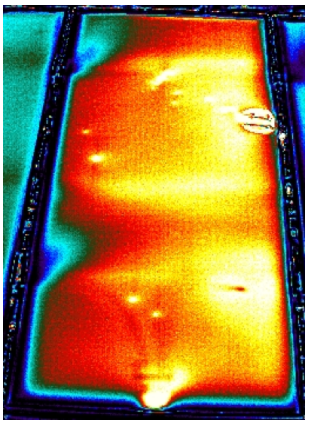

Fig. 9: Infrared image of the damaged module within string 2. The excess heating of the module has caused the string to have degraded power output.

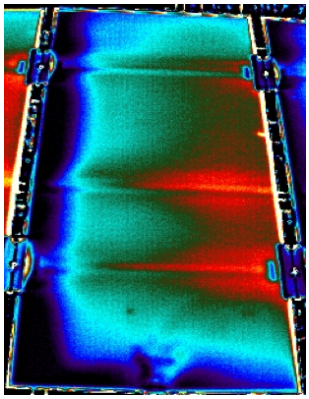

Fig. 10: Infrared image of an undamaged module within the array. The module had experienced much lower temperatures compared to the damaged one.

This paper provides a general proof of concept for the proposed methodology. It was shown that valuable information concerning PV array performance can be acquired quickly and accurately through automated and smart learning algorithms. Further investigations are necessary to review the algorithms performance for different fault and environmental conditions.

ACKNOWLEDGMENT

This work was supported by the U.S. Department of Energy SunShot Initiative

The work was also partly supported by Spanish Ministerial Commission of Science and Technology (TEC2014-52289-R) and Comunidad Autónoma de Madrid (PRICAM P2013ICE-2933) grants.

Sandia National Laboratories is a multi-program managed and operated by Sandia Corporation, a wholly owned subsidiary of Lockheed Martin Corporation, for the U.S. Department of Energy's National Nuclear Security Administration under contract DE-AC04-94AL85000

REFERENCES

[1] A. Coleman and J. Zalewski, "Intelligent fault detection and diagnostics in solar plants," in *2011 IEEE 6th International Conference on Intelligent Data Acquisition and Advanced Computing Systems (IDAACS)*, vol. 2, Sep. 2011, pp. 948–953.

[2] S. Silvestre, A. Chouder, and E. Karatepe, "Automatic fault detection in grid connected PV systems," *Solar Energy*, vol. 94, pp. 119–127, Aug. 2013. [Online]. Available: http://www.sciencedirect.com/science/article/pii/S0038092X13001849

[3] C. B. Jones, J. S. Stein, S. Gonzalez, and B. H. King, "Photovoltaic system fault detection and diagnostics using laterally primed adaptive resonance theory neural network," New Orleans, LA, USA, Jun. 2015.

[4] *Photovoltaics: Fundamentals, Technology and Practice*, 1st ed. Chichester, West Sussex, United Kingdom: Wiley, Feb. 2014.

[5] J. E. Quiroz, J. S. Stein, C. K. Carmignani, and K. Gillispie, "In-situ module-level I-V tracers for novel PV monitoring," in *Photovoltaic Specialist Conference (PVSC), 2015 IEEE 42nd*, Jun. 2015, pp. 1–6.

[6] C. Cortes and V. Vapnik, "Support-vector networks," *Machine Learning*, vol. 20, no. 3, pp. 273–297, Sep. 1995. [Online]. Available: http://link.springer.com/article/10.1007/BF00994018

[7] V. N. Vapnik, *The nature of statistical learning theory*. New York, NY, USA: Springer-Verlag New York, Inc., 1995. [Online]. Available: http://portal.acm.org/citation.cfm?id=211359

[8] A. J. Smola and B. Schölkopf, "A tutorial on support vector regression," *Statistics and Computing*, vol. 14, pp. 199–222, 2004.

[9] C. Burges, "A tutorial on support vector machines for pattern recognition," *Data Mining and Knowledge Discovery*, vol. 2, no. 2, pp. 1–32, 1998.

[10] D. Tax and R. P. W. Duin, "Support vector domain description," *Pattern Recognition Letters*, vol. 20, pp. 1191–1199, 1999.

[11] B. Schölkopf, R. C. Williamson, A. Smola, and J. Shawe-Taylor, "Support vector method for novelty detection," in *Advances in Neural Information Processing Systems 12*, Denver, CO, 1999.

[12] J. Platt, "Sequential minimal optimization: A fast algorithm for training support vector machines," p. 21, April 1998.

[13] K. P. Murphy, *Machine Learning: A Probabilistic Perspective*. MIT Press, Aug. 2012.

[14] M. A. Aizerman, E. M. Braverman, and L. I. Rozoner, "Theoretical Foundations of the Potential Function Method in Pattern Recognition Learning," *Automation and Remote Control*, vol. 25, pp. 821–837, 1964.

[15] "Pordis LLC 140a String-Level I-V Curve Tracer Specification Sheet." Pordis LLC, Tech. Rep., Jan. 2016. [Online]. Available: http://www.pordis.com/